CONTRAST MEDIA & MOLECULAR IMAGING

Received: 6 February 2015, Revised: 4 May 2015, Accepted: 25 June 2015, Published online in Wiley Online Library: 4 August 2015

(wileyonlinelibrary.com) DOI: 10.1002/cmmi.1659

PET of EGFR with ^{64}Cu-cetuximab-F(ab′)$_2$ in mice with head and neck squamous cell carcinoma xenografts

Laura K. van Dijk[a,b]*, Cheng-Bin Yim[c], Gerben M. Franssen[b], Johannes H. A. M. Kaanders[a], Johan Rajander[d], Olof Solin[c,d], Tove J. Grönroos[e], Otto C. Boerman[b] and Johan Bussink[a]

Overexpression of the epidermal growth factor receptor (EGFR) is linked to an adverse outcome in various solid tumors. Cetuximab is an EGFR inhibitor, which in combination with radiotherapy improves locoregional control and survival in a subgroup of patients with head and neck squamous cell carcinomas (HNSCCs). The aim of this study was to develop and characterize an EGFR-directed PET tracer, ^{64}Cu-cetuximab-F(ab′)$_2$, to determine the systemic accessibility of EGFR. Mice with HNSCC xenografts, UT-SCC-8 ($n = 6$) or UT-SCC-45 ($n = 6$), were imaged 24 h post injection with ^{64}Cu-NODAGA-cetuximab-F(ab′)$_2$ using PET/CT. One mouse for each tumor model was co-injected with excess unlabeled cetuximab 3 days before radiotracer injection to determine non-EGFR-mediated uptake. *Ex vivo* biodistribution of the tracer was determined and tumors were analyzed by autoradiography and immunohistochemistry. The SUV_{max} of UT-SCC-8 tumors was higher than that of UT-SCC-45: 1.5 ± 1.0 and 0.8 ± 0.2 ($p < 0.05$), respectively. SUV_{max} after *in vivo* blocking of EGFR with cetuximab was 0.4. Immunohistochemistry showed that UT-SCC-8 had a significantly higher EGFR expression than UT-SCC-45: 0.50 ± 0.19 versus 0.12 ± 0.08 ($p < 0.005$), respectively. Autoradiography indicated that ^{64}Cu-cetuximab-F(ab′)$_2$ uptake correlated with EGFR expression in both tumors: $r = 0.86 \pm 0.06$ (UT-SCC-8) and 0.90 ± 0.06 (UT-SCC-45). ^{64}Cu-cetuxmab-F(ab′)$_2$ is a promising PET tracer to determine expression of EGFR *in vivo*. Clinically, this tracer has the potential to be used to determine cetuximab targeting of tumors and possibly to non-invasively monitor the response to EGFR-inhibitor treatment.

Keywords: ^{64}Cu; EGFR; PET/CT; cetuximab; F(ab′)$_2$; HNSCC

1. INTRODUCTION

The epidermal growth factor receptor (EGFR) is a transmembranous protein linked to many regulatory cellular pathways. Its overexpression and activation can have significant effects on cellular processes and are observed in many cancers (1,2). Anti-EGFR antibodies have shown clinical activity in a variety of solid tumors including head and neck, colon, non-small-cell lung and renal cell carcinomas, thereby affecting signaling pathways leading to cell cycle arrest, apoptosis and inhibition of angiogenesis and metastasis formation (3). The EGFR is overexpressed in 80–100% of head and neck squamous cell carcinomas (HNSCCs), and the monoclonal antibody cetuximab when combined with radiotherapy has proven to be clinically effective in a small subpopulation of HNSCC patients (4,5). In order to progress to individualized treatment and reduce treatment-related toxicity, patient selection is of major clinical relevance. A well-known method for patient selection is the immunohistochemical detection of EGFR expression in biopsy-derived sections of HNSCC (6,7). However, uncertainties such as biopsy accuracy and tumor heterogeneity affect the specificity and reliability of the procedure, and results showed prognostic value but not predictive value (8). In the last decades, molecular imaging has played an important role as a noninvasive technique for patient selection, monitoring and prediction of outcome. EGFR-targeted biomarkers have been widely investigated; cetuximab and its analogues have been labeled with several radionuclides, including ^{111}In for single photon emission tomography (SPECT) and ^{124}I, ^{66}Ga, ^{89}Zr and ^{86}Y for positron emission tomography (PET) (9).

* *Correspondence to: L. K. van Dijk, Department of Radiation Oncology, Radboud University Medical Center, Nijmegen, The Netherlands. E-mail: laura.vandijk@radboudumc.nl*

a *L. K. van Dijk, J. H. A. M. Kaanders, J. Bussink*
Department of Radiation Oncology, Radboud University Medical Center, Nijmegen, The Netherlands

b *L. K. van Dijk, G. M. Franssen, O. C. Boerman*
Department of Radiology and Nuclear Medicine, Radboud University Medical Center, Nijmegen, The Netherlands

c *C.-B. Yim, O. Solin*
Radiopharmaceutical Chemistry Laboratory, Turku PET Centre, University of Turku, Turku, Finland

d *J. Rajander, O. Solin*
Accelerator Laboratory, Turku PET Centre, Åbo Akademi University, Turku, Finland

e *T. J. Grönroos*
MediCity/PET Preclinical Laboratory, Turku PET Centre, University of Turku, Turku, Finland

While whole antibodies accumulate efficiently in the tumor, it requires 4–7 days before non-target radioactivity has reached sufficiently low levels to enable acquisition of high contrast SPECT images (10). Conversely, F(ab')$_2$ fragments demonstrate high tumor-to-background signal ratios at earlier time points, while retaining tumor-binding characteristics similar to those of whole antibodies (11,12). Previous *in vivo* studies have shown that ^{111}In-cetuximab-F(ab')$_2$ can visualize EGFR accessibility in mice. It displayed a differential uptake in head and neck xenografts, with varying levels of EGFR expression and differential response to treatment with radiotherapy and/or cetuximab (13–15). The aim of this study is to develop a PET-based imaging agent with clinical perspective for imaging EGFR, as PET has a higher resolution and allows more accurate quantitative analyses of images than SPECT (16). The decay properties of ^{64}Cu include an intermediate half-life of 12.7 h, which is equal to the circulatory half-life of F(ab')$_2$ fragments. Its low positron emission energy (E_{max} = 0.65 MeV) provides high spatial resolution for PET and autoradiography (17). Therefore, the combination of PET, cetuximab-F(ab')$_2$ and ^{64}Cu creates certain potential for the clinical imaging of EGFR.

2. MATERIALS AND METHODS

2.1. Synthesis and radiochemistry

Cetuximab-F(ab')$_2$ was produced as described previously and purified by gel filtration chromatography on a G25M Sephadex column (14). Cetuximab-F(ab')$_2$ was conjugated with 2,2′-(7-(1-carboxy-4-((4-isothiocyanatobenzyl)amino)-4-oxobutyl)-1,4,7-triazonane-1,4-diyl)diacetic acid (ITC-NODAGA) (CheMatech, Dijon, France) in 0.1 M $NaHCO_3$, pH 9.5, for 3 h at room temperature using a 20-fold molar excess of ITC-NODAGA. Unbound ITC-NODAGA was removed by dialysis against NH_4OAc (0.25 M, pH 5.5).

^{64}Cu ($t_{½}$ = 12.7 h, β^+ = 17%, β^- = 39%, EC = 44%) in the form of (^{64}Cu)$CuCl_2$ was produced via the ^{64}Ni(p, n)^{64}Cu nuclear reaction, as described previously (18,19). ^{64}Cu was formulated as 5 MBq/μL in 0.04 M HCl solution. The antibody fragments (1 μg) were labeled with ^{64}Cu (5 MBq, 1 μL) in 25 μL of 2-(*N*-morpholino)ethanesulfonic acid (MES) buffer, pH 5.5 at room temperature. After 30 min, labeling efficiency was determined using instant thin-layer chromatography (ITLC) on TEC Control chromatography strips (Biodex, Shirley, NY, USA), with 0.1 M citrate buffer, pH 6.0, as the mobile phase. Radiochemical purity of ^{64}Cu-cetuximab exceeded 98% in all preparations. The specific activity of the tracer was 500 GBq/μmol.

2.2. *In vitro* characterization

^{64}Cu-cetuximab-F(ab')$_2$ (1.2 MBq, 10 μL) was added to 100 μL of murine plasma to assess stability. The mixture was incubated at 37°C. After 4 and 26 h incubation, aliquots of 1 μL were analyzed by ITLC (0.1 M citrate buffer, pH 6.0).

2.3. Tumor models

Human HNSCC UT-SCC-8 or UT-SCC-45 xenografts (1 mm^3, 1×10^6 cells) were injected in the right hind leg of male athymic BALB/*c nu/nu* mice (6–10 weeks). UT-SCC-8 originated from a supraglottic larynx and UT-SCC-45 from a primary cancer of the floor of the mouth (University of Turku). Animals were housed in filter-topped cages in a specific-pathogen-free unit in accordance with institutional guidelines. Experiments started 48 days (UT-SCC-8) or 41 days (UT-SCC-45) after transplantation. Tumor volume was estimated using the formula $(4/3)\pi r_1 r_2 r_3$. At the start of the experiment, the mean size of the tumors was 764 cm^3, with a standard error of 150 cm^3. The experiment procedures were reviewed by the Ethics Committee on Animal Experimentation of the University of Turku and approved by the Provincial State Office of Western Finland.

2.4. Biodistribution and PET/CT studies

^{64}Cu-cetuximab-F(ab')$_2$ (21 ± 2.6 MBq, 15 μg, 250 μL) was intravenously injected in the tail vein followed by 100 μL of 0.9% NaCl to flush the catheter. One additional mouse of each tumor model was injected with an excess dose of unlabeled cetuximab (1 mg) 3 days prior to tracer injection. Saturation of the antigen is often achieved by co-injection; however, as cetuximab F(ab')$_2$ targets the tumor much faster than cetuximab IgG, injection with unlabeled antibody is administered 3 days before F(ab')$_2$ tracer injection. Mice were anesthetized with 2.5% isoflurane and positioned in an Inveon PET/CT scanner (Siemens Medical Solutions, Knoxville, TN, USA) for an 8 min CT acquisition and 30 min PET scan in list mode, with an energy window of 350–650 keV. The PET scanner had an axial field of view of 12.7 cm and a spatial resolution of 1.4 mm full width at half-maximum. During scans, the body temperature of the mice was kept at 37°C with a heating pad on the scanner bed. Subsequently, mice were euthanized and the biodistribution of the radiolabel at 24 h p.i. was determined.

2.5. Immunohistochemistry and autoradiography

Frozen tumor sections (5 μm) were cut and mounted on poly-L-lysine-coated slides for autoradiography. Slides were exposed to an imaging plate (BAS-TR2025, Fuji Photo Film, Tokyo, Japan) for three days. The imaging plates were scanned using a Fuji BAS-5000 analyzer at a pixel size of 25×25 μm^2. Images were processed using a computerized image analysis program (Aida Image Analyzer software 4.19, Raytest Isotopenmessgeräte, Staubenhardt, Germany).

After autoradiography, the same slides were stained immunohistochemically. Tumor sections were fixed in acetone at 4°C for 10 min. Subsequently, sections were rehydrated in phosphate-buffered saline (PBS) and stained for EGFR. Primary and secondary antibodies were diluted in primary antibody diluent (Abcam, Cambridge, UK). Between all consecutive steps of the staining process, sections were rinsed three times each for 5 min in 0.1 M PBS, pH 7.4 (Klinipath, Duiven, The Netherlands). After rehydration in PBS, sections were incubated with goat anti-EGFR antibody 1:50 (Santa Cruz Biotechnology, Dallas, Texas, USA) and subsequently with donkey anti-goat Cy3, 1:600 (Jackson ImmunoResearch, West Grove, PA, USA), after which slides were mounted in Fluorostab (ICN, Basingstoke, UK).

2.6. Image analysis

PET images were reconstructed using an OSEM 3D algorithm of two iterations followed by maximum *a posteriori* (MAP, 18 iterations) integrative algorithms (Inveon Acquisition Workplace, version 1.5, Siemens Preclinical Solutions).

Reconstructed images were analyzed with Siemens Inveon Research Workplace software (version 4.0, Siemens Preclinical Solutions) by manually placing regions of interest (ROIs) around the tumor. Quantification of tracer uptake in tumor ROIs of the attenuation-corrected slices was obtained by calculating the maximum standardized uptake values (SUV_{max}) by correcting

for the injected activity, injection time (decay) and bodyweight. SUV_{max} was chosen as it is more reproducible than SUV_{mean}, since the maximum value within an ROI is typically less dependent on ROI position with respect to small spatial shifts.

Immunohistochemically stained tumor sections were analyzed using a digital image analysis system, as described previously (20). In short, whole-tissue sections were scanned (magnification × 10, Axioskop, Zeiss, Göttingen, Germany) and gray-scale images (pixel size, $2.59 \times 2.59\ \mu m^2$) were obtained for vessels, EGFR and nuclei, and subsequently converted into binary images. Using ImageJ software (version 1.43 m, JAVA-based image-processing package), the number of positive pixels for EGFR staining (fEGFR) was divided by total tumor area. Thresholds for segmentation of the fluorescent signals were set above the background staining for each marker. Areas of necrosis were excluded from analysis by drawing ROIs.

Colocalization analysis was performed on autoradiography and immunohistochemical gray-value images (grayscale range 0–255). Images were overlaid using Photoshop (CS4, version 11.0.2, San Jose, CA, USA), and the pixel and figure size of the immunohistochemistry images was rescaled to match that of the autoradiography images for alignment ($25 \times 25\ \mu m^2$) and was successively upscaled ($100 \times 100\ \mu m^2$) to compensate for image co-registration errors and scattering of the tracer signal in the autoradiography images. After alignment, ROIs drawn previously for excluding necrosis in immunohistochemical analysis were masked in autoradiography images. Co-registered pixel gray-values and overlap coefficients were determined with ImageJ using the JACoP plugin package (21). Positioning accuracy between the autoradiography and immunohistochemistry images, as reported by the overlap coefficient calculated with the ImageJ JACoP plugin, was over 95%.

2.7. Statistics

Statistical analyses were performed using Prism software version 6.0 (GraphPad, San Diego, CA, USA). Significance was tested with the non-parametric Mann–Whitney test and/or repeated measures ANOVA. The non-parametric Spearman or parametric Pearson test was used accordingly, and a p-value ≤ 0.05 was considered significant. Data values are represented as mean ± standard deviation.

3. RESULTS

3.1. *In vitro* characterization

^{64}Cu-cetuximab-F(ab')$_2$ was moderately stable in murine plasma. After 2 h and 26 h incubation at 37°C, 90% and 84% respectively of the radioactivity was still associated with the intact radiotracer.

3.2. Biodistribution

At 24 h p.i., the tumor biodistribution of ^{64}Cu-cetuximab-F(ab')$_2$ in the UT-SCC-8 and UT-SCC-45 xenografts was similar: 5.48 ± 1.29% ID/g and 4.23 ± 2.06% ID/g, respectively ($p = 0.36$). Mice that were pre-injected with an excess of unlabeled cetuximab had lower tumor uptake: 0.82% ID/g for UT-SCC-8 and 0.81% ID/g for UT-SCC-45. The biodistribution of ^{64}Cu-cetuximab-F(ab')$_2$ in mice with HNSCC xenografts is summarized in Fig. 1. At

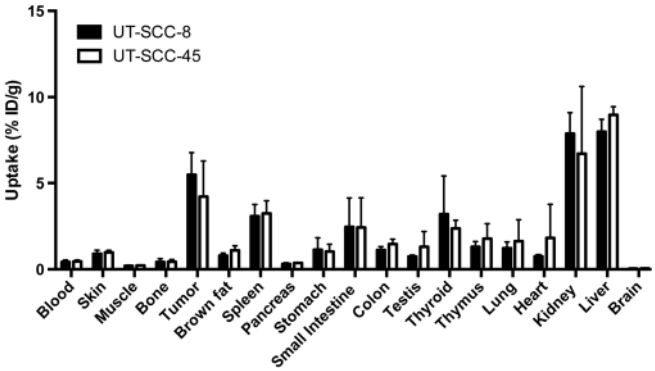

Figure 1. Biodistribution of ^{64}Cu-cetuximab-F(ab')$_2$. Black bars, mice with UT-SCC-8 ($n = 5$); white bars, mice with UT-SCC-45 ($n = 5$) tumors, 24 h p.i. Tissue uptake values are presented as percentages of injected dose per gram of tissue and expressed as mean ± SD.

24 h p.i., tumor-to-blood ratios in the two models were similar: 12.8 ± 5.2 for UT-SCC-8 and 10.6 ± 4.6 for UT-SCC-45 ($p = 0.53$). The kidneys and the liver were the normal tissues with the highest uptake: 7.9 ± 1.2% ID/g and 8.0 ± 0.7% ID/g for UT-SCC-8; 6.7 ± 3.9% ID/g and 9.0 ± 0.5% ID/g for UT-SCC-45, respectively.

3.3. PET studies

Images showed a higher^{64}Cu-cetuximab-F(ab')$_2$ uptake in UT-SCC-8 tumors than in UT-SCC-45 tumors (Fig. 2). The SUV_{max} differed significantly: 1.5 ± 1.0 for UT-SCC-8 and 0.8 ± 0.2 for UT-SCC-45 ($p < 0.05$) (Fig. 3). SUV_{max} values of the tumors of the mice pre-injected with excess unlabeled cetuximab were clearly lower: SUV_{max} was 0.4 for both UT-SCC-8 and UT-SCC-45.

3.4. Immunohistochemistry and autoradiography

UT-SCC-8 had a significantly higher expression of EGFR compared with UT-SCC-45: the receptor-positive fraction was 0.50 ± 0.19 versus 0.12 ± 0.08 ($p < 0.005$), respectively (Fig. 4). Autoradiography images of ^{64}Cu-cetuximab-F(ab')$_2$ correlated with spatial EGFR expression as determined immunohistochemically for both tumor lines: the correlation coefficient (r) was 0.86 ± 0.06 for UT-SCC-8 and 0.90 ± 0.06 for UT-SCC-45 (Fig. 5). The tumor from one mouse was omitted from the analysis owing to inability to align after skewing of the slide.

4. DISCUSSION

The present study shows that ^{64}Cu-cetuximab-F(ab')$_2$ can be used as a tracer to determine EGFR expression in HNSCCs noninvasively with PET. A significant correlation was found between the intratumoral localization of ^{64}Cu-cetuximab-F(ab')$_2$ as determined by autoradiography and EGFR expression as determined immunohistochemically, indicating that the EGFR expressed on the tumor cells is specifically targeted by the tracer.

Accumulation of ^{64}Cu-cetuximab-F(ab')$_2$ in the tumor was EGFR mediated in both UT-SCC-8 and UT-SCC-45, as it could be inhibited by pre-injection of an excess of unlabeled cetuximab. Tumor uptake of ^{64}Cu-cetuximab-F(ab')$_2$ in terms of % ID/g was similar to that of the ^{111}In-labeled cetuximab-F(ab')$_2$ tracer as described previously (13–15). Cetuximab has been radiolabeled with ^{64}Cu in several other studies, using DOTA as a chelator (22–27). However, this resulted in increased radioactivity levels

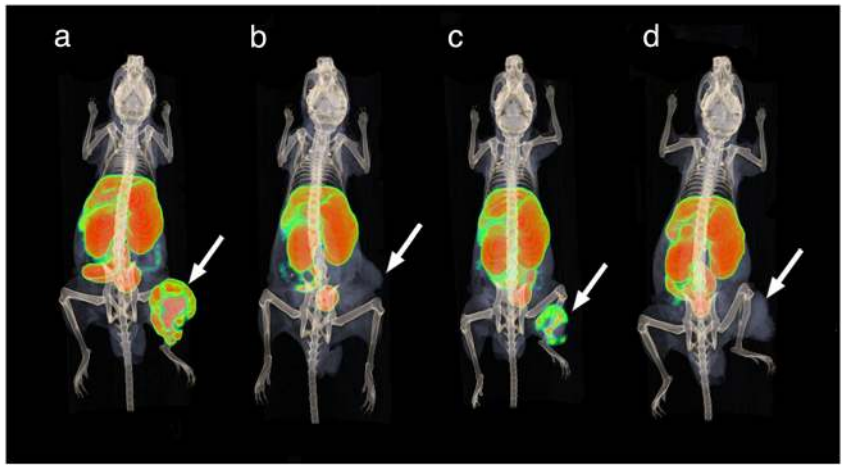

Figure 2. PET/CT images of ^{64}Cu-cetuximab-F(ab')$_2$ in mice with UT-SCC tumors. Typical examples of PET/CT images of ^{64}Cu-cetuximab-F(ab')$_2$ distribution in mice with subcutaneous UT-SCC-8 (a, b) or UT-SCC45 (c, d) tumors. b and d were pre-injected with excess cetuximab. Tumors are located subcutaneously on the right hind leg (arrow). Background uptake visible in PET images is liver, kidneys and bladder. Scans were conducted 24 h p.i.

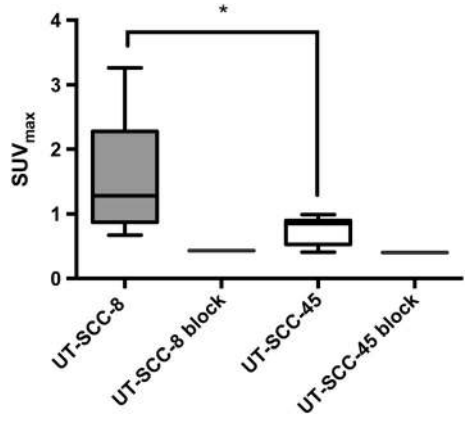

Figure 3. SUV$_{max}$ of ^{64}Cu-cetuximab-F(ab')$_2$ in UT-SCC tumors.^{64}Cu-cetuximab-F(ab')$_2$ in UT-SCC-8 ($n = 5$, grey bar) and UT-SCC-45 ($n = 5$, white bar) from PET imaging 24 h after injection. One mouse per tumor model received an excess unlabeled dose of 1 mg cetuximab 3 days prior to tracer injection (block). Data are presented as mean ± SD.* $p < 0.05$.

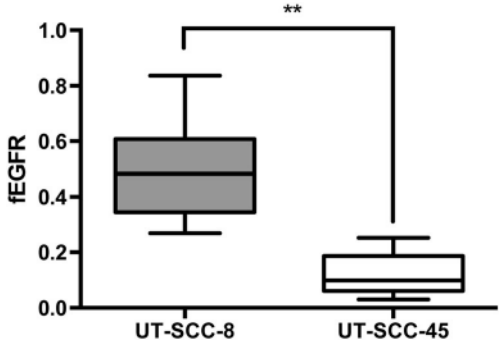

Figure 4. The immunohistochemical EGFR fraction of UT-SCC tumors. The immunohistochemical fraction of EGFR (fEGFR) of UT-SCC-8 ($n = 5$, grey bar) and UT-SCC-45 tumors ($n = 5$, white bar). UT-SCC-8 tumors had a significantly increased fEGFR ($p < 0.01$). Mean ± SD.

in the liver, which was attributed to transchelation of Cu^{2+} from DOTA to superoxide dismutase and ceruloplasmin (28). Previous reports have demonstrated the enhanced thermodynamic stability of Cu-triazamacrocyclic complexes compared with Cu-DOTA derivatives (29–35).

Yaromina *et al.* determined the TCD$_{50}$ of these UT-SCC tumors, i.e. the dose necessary to locally control 50% of the tumors, and showed that the radiosensitivities of UT-SCC-8 and UT-SCC-45 were similar, with TCD$_{50}$ values of 53 Gy and 45 Gy, respectively (36). PET images and SUV$_{max}$ quantification showed a significant difference in ^{64}Cu-cetuximab-F(ab')$_2$ uptake between the two HNSCC tumors, which might reflect the sensitivity of these tumors towards EGFR inhibitors. The ^{64}Cu-cetuximab-F(ab')$_2$ tumor uptake of UT-SCC-45 was lower, which suggests that this tumor might not benefit from EGFR-targeted therapy, while the tumor with higher tracer uptake, UT-SCC-8, might be more sensitive to EGFR inhibition. However, more HNSCC tumor models should be analyzed to validate whether tracer uptake correlates with sensitivity to cetuximab treatment.

Some discrepancy was noted between PET-derived SUV$_{max}$ and *ex vivo* biodistribution data, the latter showing no significant difference of tracer uptake in the two HNSCC tumors. The lack of a significant difference in tumor uptake could be due to necrotic areas in both UT-SCC tumor lines, thereby increasing the apparent tumor weight and distorting the uptake per gram tumor tissue, but having no effect on the SUV$_{max}$, as necrotic areas with low uptake are excluded from that analysis.

In a previous study, ^{111}In-cetuximab-F(ab')$_2$ has been shown to be able to measure radiation-induced changes of EGFR expression. Irradiated SCCNij202 tumors exhibited an increase in ^{111}In-cetuximab-F(ab')$_2$ uptake up to 14 days after treatment, which correlated with an increase of available membranous EGFR as determined immunohistochemically (15). Intratumoral localization of EGFR in HNSCCs is heterogeneous, and to allow accurate tracer quantification and reduction of partial volume effects it is necessary to acquire high-resolution images. Clinical PET images have a better spatial resolution than SPECT images (2–5 mm versus 7–10 mm), encouraging the development of PET tracers for this application (16). The ability of ^{64}Cu-cetuximab-F(ab')$_2$ to monitor treatment has not yet been established, but the current study shows that this PET tracer is able to accurately measure heterogeneous EGFR expression in tumors within a relatively short time period.

Optimization of kinetics and specificity of PET tracers is necessary in order to advance in a clinical setting. Longitudinal

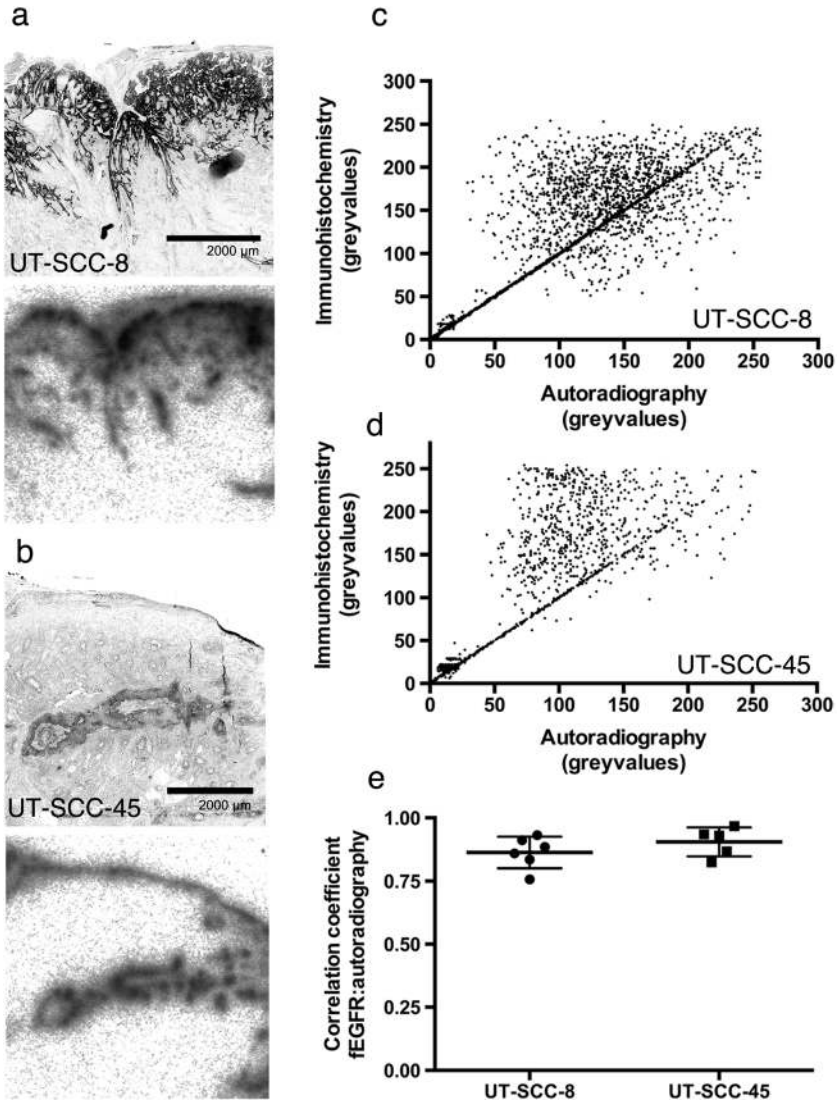

Figure 5. Correlation of EGFR immunohistochemistry and ^{64}Cu-cetuximab-F(ab′)$_2$ autoradiography. (a–d) UT-SCC-8 EGFR immunohistochemistry image (top) and corresponding autoradiography (bottom) (a), immunohistochemistry image of UT-SCC-45 (top) and corresponding autoradiography (bottom) (b) and their respective correlations (c, d). (e) The intratumoral distribution of ^{64}Cu-cetuximab-F(ab′)$_2$ as determined by autoradiography correlated well with the immunohistochemical distribution of EGFR ($r = 0.88$, range 0.76–0.97), mean ± SD. Magnification × 10. Bars: 2000 µm.

measurement of EGFR expression could elucidate patient-specific tumor characteristics during the course of the disease and during treatment, thereby facilitating personalized treatment. The preclinical data described here suggest the potential of ^{64}Cu-cetuximab-F(ab′)$_2$ as a clinical EGFR-targeting tracer.

5. CONCLUSION

This report described the successful NODAGA conjugation and ^{64}Cu labeling of cetuximab-F(ab′)$_2$ with high specific radioactivity. PET studies showed the potential of the ^{64}Cu-cetuximab-F(ab′)$_2$ radiotracer to determine systemically targetable EGFR expression in heterogeneous tumors with superior image quality at a relatively early time interval. The tracer accumulated rapidly in two different HNSCC tumor models with good tumor-to-background signal at 24 h after injection. Tracer uptake in the tumor models studied correlated to EGFR expression as measured by immunohistochemistry. Imaging with the PET tracer ^{64}Cu-cetuxmab-F(ab′)$_2$ shows clinical promise in determining intratumoral EGFR distribution, and might predict cetuximab accumulation and subsequent response to EGFR-inhibitor treatment.

Acknowledgements

The authors thank Jasper Lok, Wenny Peeters and Peter Laverman (Radboud University Medical Center) and Francisco Lopez, Aake Honkaniemi, Jaakko Lehtimaki, Marko Vehmanen and Elisa Riuttala (University of Turku) for their technical assistance.

Financial support: Dutch Cancer Society, grant no NKB-KUN 2010-4688. Part of this study was conducted within the Finnish Centre of Excellence in Molecular Imaging in Cardiovascular and Metabolic Research, financially supported by the Academy of Finland, University of Turku, Turku University Hospital and Åbo Akademi University.

REFERENCES

1. Nijkamp MM, Span PN, Bussink J, Kaanders JH. Interaction of EGFR with the tumour microenvironment: implications for radiation treatment. Radiother Oncol 2013; 108(1): 17–23.
2. Bussink J, van der Kogel AJ, Kaanders JH. Activation of the PI3-K/AKT pathway and implications for radioresistance mechanisms in head and neck cancer. Lancet Oncol 2008; 9(3): 288–296.
3. Mendelsohn J, Baselga J. Epidermal growth factor receptor targeting in cancer. Semin Oncol 2006; 33(4): 369–385.
4. Bonner JA, Harari PM, Giralt J, Azarnia N, Shin DM, Cohen RB, Jones CU, Sur R, Raben D, Jassem J, Ove R, Kies MS, Baselga J, Youssoufian H, Amellal N, Rowinsky EK, Ang KK. Radiotherapy plus cetuximab for squamous-cell carcinoma of the head and neck. N Engl J Med 2006; 354(6): 567–578.
5. Harari PM. Epidermal growth factor receptor inhibition strategies in oncology. Endocr Relat Cancer 2004; 11(4): 689–708.
6. Bentzen SM, Atasoy BM, Daley FM, Dische S, Richman PI, Saunders MI, Trott KR, Wilson GD. Epidermal growth factor receptor expression in pretreatment biopsies from head and neck squamous cell carcinoma as a predictive factor for a benefit from accelerated radiation therapy in a randomized controlled trial. J Clin Oncol 2005; 23(24): 5560–5567.
7. Chung KY, Shia J, Kemeny NE, Shah M, Schwartz GK, Tse A, Hamilton A, Pan D, Schrag D, Schwartz L, Klimstra DS, Fridman D, Kelsen DP, Saltz LB. Cetuximab shows activity in colorectal cancer patients with tumors that do not express the epidermal growth factor receptor by immunohistochemistry. J Clin Oncol 2005; 23(9): 1803–1810.
8. Keren S, Shoude Z, Lu Z, Beibei Y. Role of EGFR as a prognostic factor for survival in head and neck cancer: a meta-analysis. Oncodevelopmental Biol Med 2014; 35(3): 2285–2295.
9. Sihver W, Pietzsch J, Krause M, Baumann M, Steinbach J, Pietzsch HJ. Radiolabeled cetuximab conjugates for EGFR targeted cancer diagnostics and therapy. Pharmaceuticals 2014; 7(3): 311–338.
10. Hoeben BA, Molkenboer-Kuenen JD, Oyen WJ, Peeters WJ, Kaanders JH, Bussink J, Boerman OC. Radiolabeled cetuximab: dose optimization for epidermal growth factor receptor imaging in a head-and-neck squamous cell carcinoma model. Int J Cancer 2011; 129(4): 870–878.
11. Heskamp S, van Laarhoven HW, Molkenboer-Kuenen JD, Bouwman WH, van der Graaf WT, Oyen WJ, Boerman OC. Optimization of IGF-1R SPECT/CT imaging using ^{111}In-labeled F(ab')(2) and Fab fragments of the monoclonal antibody R1507. Mol Pharm 2012; 9(8): 2314–2321.
12. Hoeben BA, Kaanders JH, Franssen GM, Troost EG, Rijken PF, Oosterwijk E, van Dongen GA, Oyen WJ, Boerman OC, Bussink J. PET of hypoxia with ^{89}Zr-labeled cG250-F(ab')$_2$ in head and neck tumors. J Nucl Med 2010; 51(7): 1076–1083.
13. van Dijk LK, Hoeben BA, Stegeman H, Kaanders JH, Franssen GM, Boerman OC, Bussink J. ^{111}In-cetuximab-F(ab')$_2$ SPECT imaging for quantification of accessible epidermal growth factor receptors (EGFR) in HNSCC xenografts. Radiother Oncol 2013; 108(3): 484–488.
14. van Dijk LK, Hoeben BA, Kaanders JH, Franssen GM, Boerman OC, Bussink J. Imaging of epidermal growth factor receptor expression in head and neck cancer with SPECT/CT and ^{111}In-labeled cetuximab-F(ab')$_2$. J Nucl Med 2013; 54(12): 2118–2124.
15. van Dijk LK, Boerman OC, Franssen GM, Lok J, Kaanders JH, Bussink J. Early response monitoring with ^{18}F-FDG PET and cetuximab-F(ab')$_2$-SPECT after radiotherapy of human head and neck squamous cell carcinomas in a mouse model. J Nucl Med 2014; 55(10): 1665–1670.
16. Histed SN, Lindenberg ML, Mena E, Turkbey B, Choyke PL, Kurdziel KA. Review of functional/anatomical imaging in oncology. Nucl Med Commun 2012; 33(4): 349–361.
17. Covell DG, Barbet J, Holton OD, Black CD, Parker RJ, Weinstein JN. Pharmacokinetics of monoclonal immunoglobulin G_1, F(ab')$_2$, and Fab' in mice. Cancer Res 1986; 46(8): 3969–3978.
18. Rajander J, Schlesinger J, Avila-Rodriguez MA, Solin O. Increasing specific activity in Cu-64 production by reprocessing the Ni-64 target material. J Labelled Comp Radiopharm 2009; 52: S234–S234.
19. McCarthy DW, Shefer RE, Klinkowstein RE, Bass LA, Margeneau WH, Cutler CS, Anderson CJ, Welch MJ. Efficient production of high specific activity ^{64}Cu using a biomedical cyclotron. Nucl Med Biol 1997; 24(1): 35–43.
20. Rademakers SE, Rijken PF, Peeters WJ, Nijkamp MM, Barber PR, van der Laak J, van de Kogel AJ, Bussink J, Kaanders JH. Parametric mapping of immunohistochemically stained tissue sections; a method to quantify the colocalization of tumor markers. Cell Oncol 2011; 34(2): 119–129.
21. Bolte S, Cordelieres FP. A guided tour into subcellular colocalization analysis in light microscopy. J Microsc 2006; 224(Pt 3): 213–232.
22. Achmad A, Hanaoka H, Yoshioka H, Yamamoto S, Tominaga H, Araki T, Ohshima Y, Oriuchi N, Endo K. Predicting cetuximab accumulation in *KRAS* wild-type and *KRAS* mutant colorectal cancer using ^{64}Cu-labeled cetuximab positron emission tomography. Cancer Sci 2012; 103(3): 600–605.
23. Eiblmaier M, Meyer LA, Watson MA, Fracasso PM, Pike LJ, Anderson CJ. Correlating EGFR expression with receptor-binding properties and internalization of ^{64}Cu-DOTA-cetuximab in 5 cervical cancer cell lines. J Nucl Med 2008; 49(9): 1472–1479.
24. Sadri K, Ren Q, Zhang K, Paudyal B, Devadhas D, Rodeck U, Thakur M. PET imaging of EGFR expression in nude mice bearing MDA-MB-468, a human breast adenocarcinoma. Nucl Med Commun 2011; 32(7): 563–569.
25. Ping Li W, Meyer LA, Capretto DA, Sherman CD, Anderson CJ. Receptor-binding, biodistribution, and metabolism studies of ^{64}Cu-DOTA-cetuximab, a PET-imaging agent for epidermal growth-factor receptor-positive tumors. Cancer Biother Radiopharm 2008; 23(2): 158–171.
26. Cai W, Chen K, He L, Cao Q, Koong A, Chen X. Quantitative PET of EGFR expression in xenograft-bearing mice using ^{64}Cu-labeled cetuximab, a chimeric anti-EGFR monoclonal antibody. Eur J Nucl Med Mol Imaging 2007; 34(6): 850–858.
27. Guo Y, Parry JJ, Laforest R, Rogers BE, Anderson CJ. The role of p53 in combination radioimmunotherapy with ^{64}Cu-DOTA-cetuximab and cisplatin in a mouse model of colorectal cancer. J Nucl Med 2013; 54(9): 1621–1629.
28. Wadas TJ, Wong EH, Weisman GR, Anderson CJ. Copper chelation chemistry and its role in copper radiopharmaceuticals. Curr Pharm Des 2007; 13(1): 3–16.
29. Roosenburg S, Laverman P, Joosten L, Cooper MS, Kolenc-Peitl PK, Foster JM, Hudson C, Leyton J, Burnet J, Oyen WJ, Blower PJ, Mather SJ, Boerman OC, Sosabowski JK. PET and SPECT imaging of a radiolabeled minigastrin analogue conjugated with DOTA, NOTA, and NODAGA and labeled with Cu, Ga, and In. Mol Pharm 2014; 11 (11): 3930–3937.
30. Prasanphanich AF, Nanda PK, Rold TL, Ma L, Lewis MR, Garrison JC, Hoffman TJ, Sieckman GL, Figueroa SD, Smith CJ. [^{64}Cu-NOTA-8-Aoc-BBN(7-14)NH_2] targeting vector for positron-emission tomography imaging of gastrin-releasing peptide receptor-expressing tissues. Proc Natl Acad Sci U S A 2007; 104(30): 12462–12467.
31. Kukis DL, Li M, Meares CF. Selectivity of antibody–chelate conjugates for binding copper in the presence of competing metals. Inorg Chem 1993; 32(19): 3981–3982.
32. Kukis DL, Diril H, Greiner DP, Denardo SJ, Denardo GL, Salako QA, Meares CF. A comparative-study of copper-67 radiolabeling and kinetic stabilities of antibody–macrocycle chelate conjugates. Cancer 1994; 73(3): 779–786.
33. Fani M, Del Pozzo L, Abiraj K, Mansi R, Tamma ML, Cescato R, Waser B, Weber WA, Reubi JC, Maecke HR. PET of somatostatin receptor-positive tumors using ^{64}Cu- and ^{68}Ga-somatostatin antagonists: the chelate makes the difference. J Nucl Med 2011; 52(7): 1110–1118.
34. Banerjee SR, Pullambhatla M, Foss CA, Nimmagadda S, Ferdani R, Anderson CJ, Mease RC, Pomper MG. ^{64}Cu-labeled inhibitors of prostate-specific membrane antigen for PET imaging of prostate cancer. J Med Chem 2014; 57(6): 2657–2669.
35. Ait-Mohand S, Fournier P, Dumulon-Perreault V, Kiefer GE, Jurek P, Ferreira CL, Benard F, Guerin B. Evaluation of ^{64}Cu-labeled bifunctional chelate–bombesin conjugates. Bioconjug Chem 2011; 22(8): 1729–1735.
36. Yaromina A, Krause M, Thames H, Rosner A, Krause M, Hessel F, Grenman R, Zips D, Baumann M. Pre-treatment number of clonogenic cells and their radiosensitivity are major determinants of local tumour control after fractionated irradiation. Radiother Oncol 2007; 83(3): 304–310.